Ellipsometric characterization and density-functional theory analysis of anisotropic optical properties of single-crystal -SnS

R. E. Banai, L. A. Burton, S. G. Choi, F. Hofherr, T. Sorgenfrei, A. Walsh, B. To, A. Cröll, and J. R. S. Brownson

Citation: Journal of Applied Physics **116**, 013511 (2014); doi: 10.1063/1.4886915
View online: http://dx.doi.org/10.1063/1.4886915
View Table of Contents: http://scitation.aip.org/content/aip/journal/jap/116/1?ver=pdfcov
Published by the AIP Publishing

JOURNAL OF APPLIED PHYSICS **116**, 013511 (2014)

Ellipsometric characterization and density-functional theory analysis of anisotropic optical properties of single-crystal α-SnS

R. E. Banai,[1] L. A. Burton,[2] S. G. Choi,[3,a)] F. Hofherr,[4] T. Sorgenfrei,[4] A. Walsh,[2] B. To,[3] A. Cröll,[4] and J. R. S. Brownson[1]
[1]*Department of Materials Science and Engineering, Pennsylvania State University, University Park, Pennsylvania 16802, USA*
[2]*Centre for Sustainable Chemical Technologies and Department of Chemistry, University of Bath, Claverton Down, Bath BA2 7AY, United Kingdom*
[3]*National Renewable Energy Laboratory, Golden, Colorado 80401, USA*
[4]*Crystallography—Institute of Earth and Environmental Sciences, University of Freiburg, 79104 Freiburg, Germany*

(Received 17 April 2014; accepted 23 June 2014; published online 7 July 2014)

We report on the anisotropic optical properties of single-crystal tin monosulfide (SnS). The components ε_a, ε_b, and ε_c of the pseudodielectric-function tensor $\langle\varepsilon\rangle = \langle\varepsilon_1\rangle + i\langle\varepsilon_2\rangle$ spectra are taken from 0.73 to 6.45 eV by spectroscopic ellipsometry. The measured $\langle\varepsilon\rangle$ spectra are in a good agreement with the results of the calculated dielectric response from hybrid density functional theory. The $\langle\varepsilon\rangle$ spectra show the direct band-gap onset and a total of eight above-band-gap optical structures that are associated with the interband-transition critical points (CPs). We obtain accurate CP energies by fitting analytic CP expressions to second-energy-derivatives of the $\langle\varepsilon\rangle$ data. Their probable electronic origins and implications for photovoltaic applications are discussed. © *2014 AIP Publishing LLC*. [http://dx.doi.org/10.1063/1.4886915]

I. INTRODUCTION

A natural *p*-type IV–VI binary compound tin monosulfide (SnS) is considered a promising absorber material for the next-generation thin-film photovoltaic (PV) technology. SnS has a suitable band-gap energy of ~1.1 eV,[1] a large optical absorption coefficient of 10^4–10^5 cm^{-1} above the band gap,[2,3] a high intrinsic free carrier concentration of ~10^{17} cm^{-3},[4] and earth abundance of the constituent elements. These properties suggest that PV devices with efficiencies as high as 24% are possible.[5]

Despite material properties that are almost ideal for PV device applications, the power conversion efficiency (η) of SnS solar cells is so far limited to 4.4%,[6] which is substantially smaller than the values achieved with alternate materials with similar opto-electronic properties.[7] In attempts to increase the η of SnS solar cells, crystalline quality has been improved,[8] optimum device architecture has been suggested,[9] and detrimental effects of the possible secondary phases, such as SnS_2 and Sn_2S_3, on the device performance have been examined.[10]

Knowledge of optical properties of materials plays an important role in the development of high-efficiency solar cells.[11–13] Complex refractive index $N = n + ik$ and relevant properties, such as normal-incidence reflectivity R and absorption coefficient α, are used to characterize the device performance.[14,15] The complex dielectric function $\varepsilon = \varepsilon_1 + i\varepsilon_2$ provides great insight into the electronic structure of materials and can be used to compare experimental data to theoretical predictions,[16–19] which in turn further enhances the performance and functionality of solar cells through *band gap*- and *defect-engineering*.

For SnS, however, clear discrepancies exist among the reported optical data of polycrystalline thin films.[3,20–30] In addition, optical properties of reference single-crystal SnS have not been well established, yet. The layer-structured SnS crystallizes in the orthorhombic structure (space group *Pnma*) with the lattice parameters of $a = 4.33$ Å, $b = 3.98$ Å, and $c = 11.18$ Å,[31] which is depicted in Fig. 1. Therefore, SnS is expected to exhibit anisotropy in its optical properties. The ε_a and ε_b spectra have been derived from a combined analysis of optical transmission and electron-energy-loss spectra from 0.5 to 22 eV.[32] The N spectra for a single-crystal SnS, determined by unpolarized transmission measurements,[33] also showed optical anisotropy along the a and b principal axes. However, details of the optical structures shown in ε_a and ε_b spectra have not been discussed and the experimental spectrum for ε_c is still not available in the literature.

Here, we apply spectroscopic ellipsometry (SE) to determine the room-temperature pseudodielectric function $\langle\varepsilon_a\rangle$, $\langle\varepsilon_b\rangle$, and $\langle\varepsilon_c\rangle$ spectra for single-crystal SnS. The SE results show a good agreement with the ε_a, ε_b, and ε_c data calculated by hybrid density functional theory (DFT). In addition to the band-gap onset, a total of eight optical structures associated with the interband-transition critical points (CPs) are shown in the $\langle\varepsilon\rangle$ spectra, and the CP energy values are accurately obtained from the standard line-shape analysis[34,35] of the numerically calculated $d^2\langle\varepsilon\rangle/dE^2$ data. Electronic origins of CP energies and implications for PV device applications are discussed.

II. EXPERIMENTS

A single crystal SnS bulk was grown by the Bridgman-Stockbarger technique in a sealed fused silica glass ampoule.

a)Author to whom correspondence should be addressed. Electronic mail: sukgeun.choi@nrel.gov.

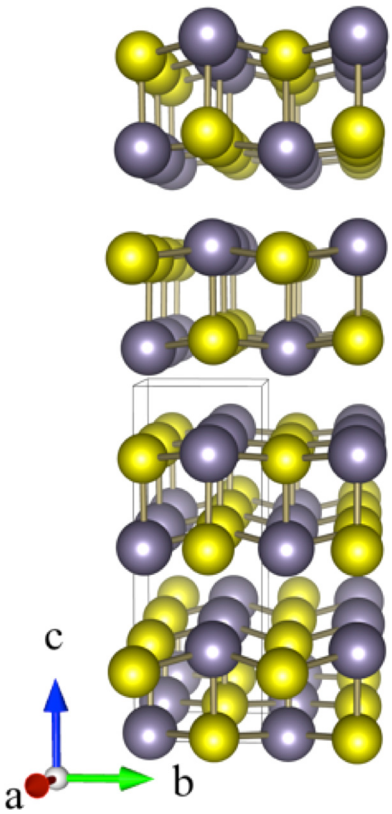

FIG. 1. The distorted-rocksalt orthorhombic (*Pnma*) crystal structure of SnS. The Sn atoms are colored dark grey.

As starting material, poly-crystal of an *ab-initio* synthesis in a stoichiometric composition was used. The bulk growth was done in a vertical resistance furnace consisting of three independent heating zones. Before growth, the material was homogenized for 1 hr. in zone 1 at 930 °C, which is above the melting point of 880 °C. During the growth, the temperature gradient (ΔT) was 13°/cm and the growth rate was 0.5 mm/h. Details of the growth and structural characterization are given in Ref. 36.

For SE measurements, a 2 mm-thick slab was cut from the bulk crystal with a large surface (approximately 100 mm^2) normal to the *c* direction. The large surface consisting of *a* and *b* axes and one side-face containing *b* and *c* axes were chemo-mechanically polished to reduce the surface overlayer artifacts. Diamond lapping films with various grit sizes ranging from 30 to 0.1 μm were used in an Allied High Tech Multi Purpose polishing system to progressively polish the surface, and the procedure was completed in conjunction with a 0.05–μm colloidal silica suspension applied on a polishing cloth. The crystallographic orientations of the sample were determined by the Laue diffraction measurements. The polishing procedure results in a small discrepancy between the actual measurement surfaces and ideal crystallographic planes, which, estimated from modeling of the SE data, were 0.42°, 0.39°, and 0.35° for the planes normal to the *a*, *b*, and *c* axes, respectively.

SE measurements were performed in the spectral range of 0.73 to 6.45 eV with the sample maintained at room temperature using a spectroscopic rotating compensator-type ellipsometer (J.A. Woollam Inc., M2000-DI model). The angle of incidence was 70°. The polarizer was set to 45° while the analyzer angle was switched between +45° and −45°. SE data were recorded after taking an average of the results obtained at two analyzer angles (zone averaging) to improve the accuracy.

The contribution from the ε tensor component along the axis normal to the measurement surface is known to be negligible to the SE data, which is reduced approximately by $1/\varepsilon$.[37] On the other hand, the SE measurement is most sensitive to the ε tensor component aligned to the intersecting line drawn by sample surface and plain of incidence (POI).[37,38] For the SnS crystal used in this study, the *c*-axis is normal to the measurement surface, while the *a* and *b* axes are embedded within the surface. Hence, the ε_a and ε_b spectra can be acquired by rotating the sample about the surface normal, such that the intersecting line (i.e., POI) is parallel to the *a*- and *b*-axis, respectively, as depicted in Fig. 2(a). Similarly, the ε_c spectrum can be obtained by taking SE data on a side face of the SnS crystal with the *c* axis parallel to the intersecting line (Fig. 2(b)).

For the actual SE measurements, the POI was roughly aligned to the predetermined principal axis using a manual rotating sample stage with the angular precision better than ±0.5°. A fine adjustment was made by rotating the crystal to the angular position where the contributions from the off-diagonal components of the Jones matrix become negligible in the anisotropic SE data.[39] Thus, the generalized ellipsometry[40] is not critically required here and the $\langle\varepsilon_a\rangle$, $\langle\varepsilon_b\rangle$, and $\langle\varepsilon_c\rangle$ spectra reported in this work are a good approximation to the intrinsic ε spectra for the corresponding components with the minimum "cross-talk" among the three components.

III. COMPUTATIONAL DETAILS

The electronic structure of SnS was calculated within DFT using a non-local hybrid exchange-correlation functional developed by Heyd, Scuseria, and Ernzerhof (HSE06).[41] All calculations were performed using the Vienna *Ab-initio* Simulation Package (VASP) code,[42] with the projector augmented wave (PAW) approach,[43] a 400 eV plane wave cut-off, and reciprocal space sampling of $6 \times 6 \times 4$ *k*-points. The calculations included 240 bands, 40 of which were occupied. Electronic densities of states were calculated using the tetrahedron method with Blöchl corrections.

The structural parameters of SnS were fixed at the experimentally determined room-temperature values of

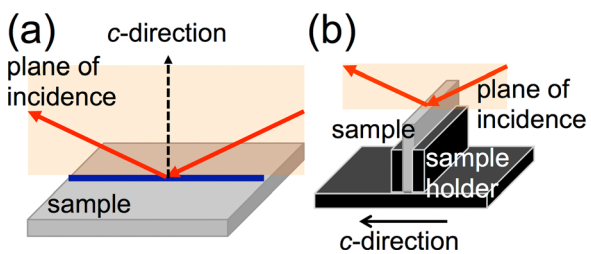

FIG. 2. Schematics depicting the SE measurements of (a) the large measurement surface containing the *a* and *b* axes, and (b) the polished side-face containing the *c* axis. A plane of incidence is indicated as the shaded area. For the SE measurement of the side-face, a homemade spring-loaded sample holder was used.

Ref. 44 in order to avoid errors associated with temperature and van der Waals interactions, which are not negligible in this pseudo-layered structure. Values of effective mass were calculated using the electronic structure module of the pymatgen library,[45] in conjunction with the BoltzTrap code.[46] The image of SnS chemical structure was made using VESTA software.[47]

The $\varepsilon(\omega)$ was calculated within the electric dipole approximation from the real and imaginary hybrid Kohn-Sham eigenstates.[48] The imaginary part of the frequency dependent dielectric response is computed by

$$\varepsilon_2(\omega) = 1 + \frac{4\pi^2 e^2}{\Omega} \lim_{q\to 0} \frac{1}{q^2} \sum_{c,\upsilon,k} 2\omega_k \delta(\varepsilon_{ck} - \varepsilon_{\upsilon k} - \omega) \times u_{ck+c_\alpha q} | u_{\upsilon k} u_{ck+c\beta q} | u_{\upsilon k}, \quad (1)$$

where c and υ refer to the conduction and valence band states, respectively, and u_{ck} is the cell periodic part of the orbitals at the k-point k. ω is the frequency of the incident photon and Ω is the volume of the unit cell. The real part of the dielectric tensor is obtained using the standard Kramers-Krönig transformation

$$\varepsilon_1(\omega) = 1 + \frac{2}{\pi} P \int_0^\infty \frac{\varepsilon_r^{(2)}(\omega')\omega'}{\omega'^2 - \omega^2 + i\eta} d\omega', \quad (2)$$

where P denotes the principal value and η is the complex shift.

IV. RESULTS AND DISCUSSION

The calculated electronic band structure of SnS is shown in Fig. 3. With the HSE06 treatment of electron exchange and correlation, SnS exhibits a fundamental electronic band gap of 1.11 eV that is spatially indirect, and a direct gap of 1.22 eV. Although the SE data do not resolve it due to low transition intensities, the prediction of indirect gap at 1.11 eV is consistent with the results from other theoretical[28,49] and experimental[20,50] studies.

The electronic band dispersion of SnS is typical of a layered material with a relatively flat band structure associated with the weakly interacting layers (longer Sn–S interatomic separation) and more dispersive pattern in the strongly bonded plane. The effective mass tensor from the integrated average of the second derivative of the band structure is reported, taking into account non-parabolicity and multiple bands and extrema. For this level of theory and a typical p-type dopant concentration of 1×10^{17} cm^{-3},[4,22] the values of effective mass are 1.17, 0.24, and 1.61 for holes and 0.67, 0.30, and 0.36m_0 for electrons in the a, b, and c directions, respectively. Experimental effective masses for holes along the b crystallographic orientation determined by free carrier reflectivity measurements are also of the order of 0.2m_0.[51] These results show a strong preference for charge transport in the b direction for both carrier types.

Calculated and SE-determined ε_a, ε_b, and ε_c spectra are presented in Figs. 4(a)–4(f), showing a good agreement in the overall shape. The calculated dielectric constants along

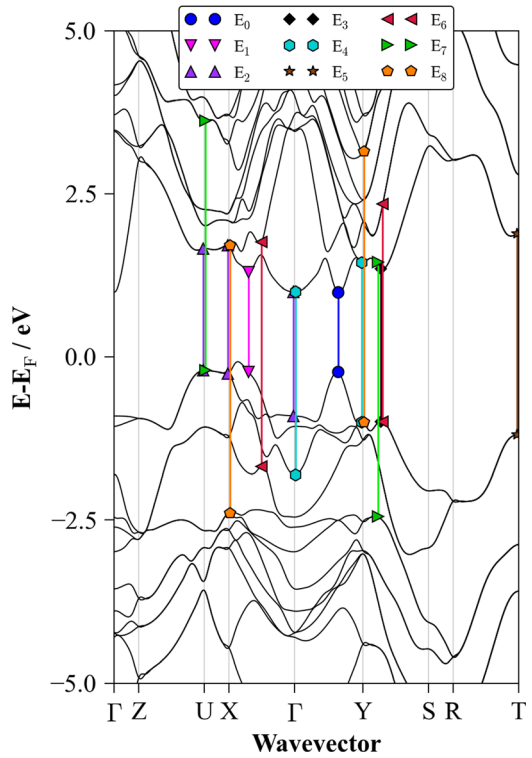

FIG. 3. The calculated electronic energy band structure of SnS. The major critical points are identified at various symmetric points of Brillouin zone.

the a, b, and c principal axes are listed in Table I. The calculated optical dielectric constants ε_∞ are in a good agreement with the SE-determined $\langle\varepsilon_1\rangle$ values at the low energy limit: 12.82 for $\langle\varepsilon_a\rangle$, 15.97 for $\langle\varepsilon_b\rangle$, and 13.25 for $\langle\varepsilon_c\rangle$. We note that the SE data shown in Figs. 4(b), 4(d), and 4(f) are *pseudodielectric function*[52] $\langle\varepsilon\rangle = \langle\varepsilon_1\rangle + i\langle\varepsilon_2\rangle$ spectra that are the direct inversion of experimental data, where no mathematical data modeling is involved. Nonzero $\langle\varepsilon_2\rangle$ value below ~1.3 eV can be thus a result of indirect band-gap nature of SnS crystal, a possible presence of thin surface overlayers such as native oxides and microscopic roughness, or a combination of the preceding. Owing to the uncertainty in the origin of below-band-gap absorption, we did not attempt a multilayer analysis in this study and report the $\langle\varepsilon\rangle$ spectra that have been taken after careful surface preparation procedures.

The SE-determined $\langle\varepsilon_a\rangle$ and $\langle\varepsilon_b\rangle$ spectra are in a good agreement with the data obtained from a combined analysis of optical transmission and electron-energy-loss spectra.[32] The ε_{a2} spectra (Figs. 4(a) and 4(b)) show one broad optical structure with several fine features spanning from ~1.3 to ~5.0 eV. As an example, the major above-band-gap CP structures are identified based on the results of calculated electronic energy band structure (Fig. 3) in Fig. 4(a).

In conjunction with the assigned probable vertical transitions (Fig. 3), we can elucidate the origin of the observed optical transitions. The ε_{b2} spectra (Figs. 4(c) and 4(d)) can be characterized by a large optical structure at ~2.5 eV followed by a weak broad structure centered at ~4 eV. The electronic origin of the main peak at ~2.5 eV can be identified as a transition primarily from S p and Sn s orbitals in the valence band to Sn p orbitals in the conduction band

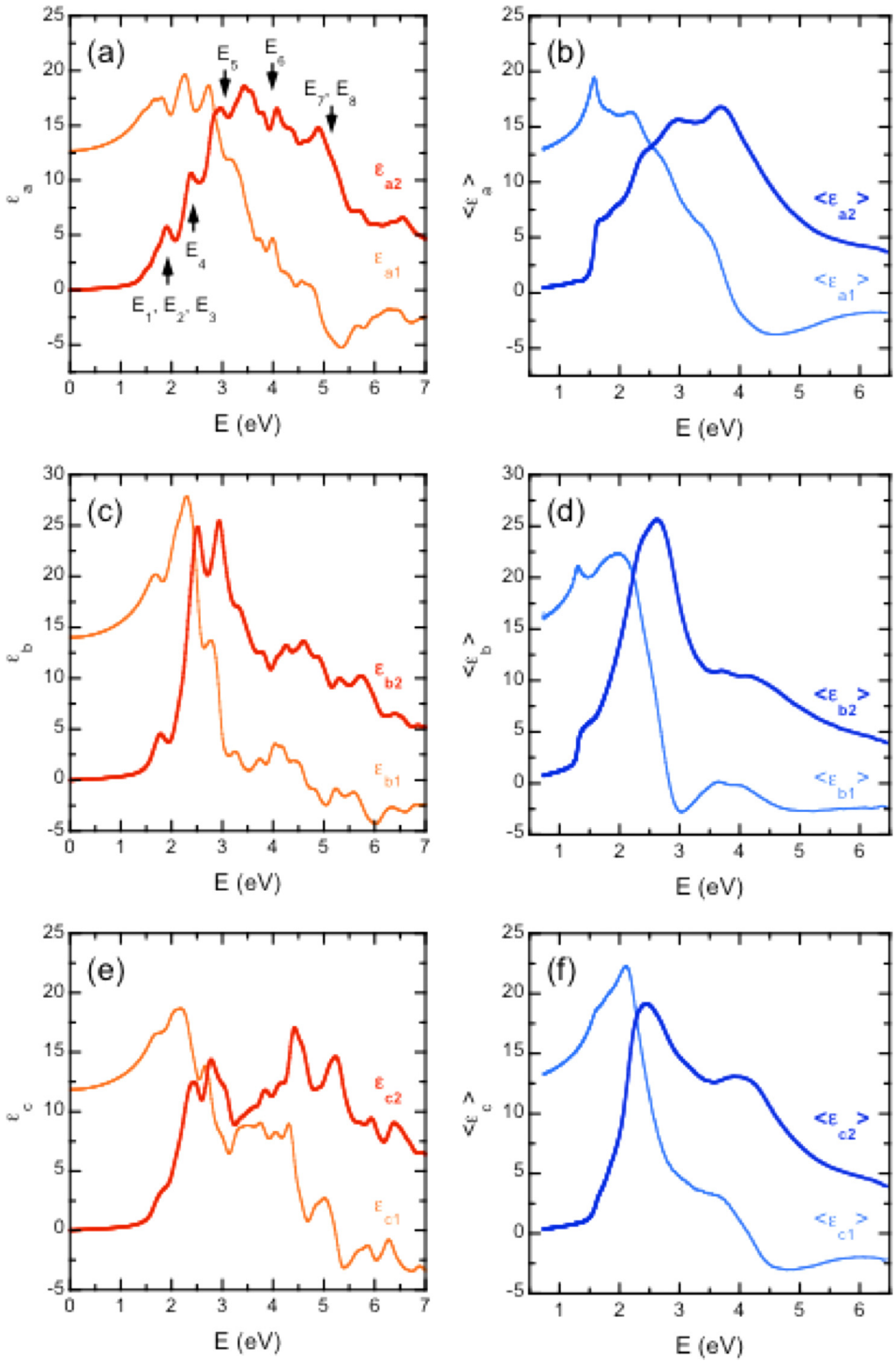

FIG. 4. Calculated and SE-determined ε spectra for the a (a,b), b (c,d), and c (e,f) principal axes. Calculated data are presented in the left column (a, c, and e) and SE-determined $<\varepsilon>$ spectra are shown in the right column (b, d, and f), respectively. Real part (ε_1) and imaginary part (ε_2) are shown as light-thin and dark-thick lines, respectively.

TABLE I. Calculated high frequency (ε_∞) and static (ε_0) dielectric constants of SnS (from HSE06-DFT). The ionic contribution to the response is calculated using the phonon dispersion from density functional perturbation theory.

Property	ε_a	ε_b	ε_c
$\varepsilon_{\text{ionic}}$	21.36	37.64	22.72
ε_∞	12.70	14.02	11.85
$\varepsilon_0 = \varepsilon_\infty + \varepsilon_{\text{ionic}}$	34.06	51.66	34.57

occurring between the Γ and Y points in the Brillouin zone (BZ). The high density of transitions within this narrow region of the BZ at similar energies accounts for the comparatively stronger absorption profile in the b direction. For the ε_{c2} spectra (Figs. 4(e) and 4(f)), two distinct structures are seen at ∼2.5 and ∼4 eV whose electronic origins are understood to be the same as those observed in the ε_{b2} spectra. No experimental ε_c spectrum for SnS is available in the literature to compare with our ε_{c2} data, but the calculations reported by Makinistian and Albanesi[53] show similar results.

The direct band-gap energy is one of the key optical parameters of materials for the applications in PV devices.

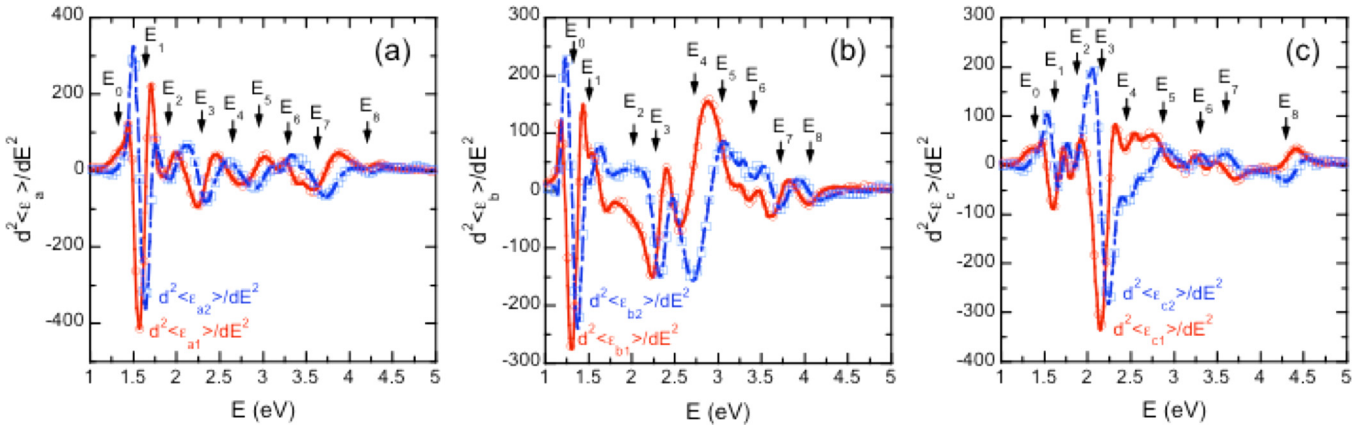

FIG. 5. Red solid and blue dashed-dotted lines: standard CP lineshapes best fit to second-energy-derivatives $d^2\langle\varepsilon_1\rangle/dE^2$ (open circles) and $d^2\langle\varepsilon_2\rangle/dE^2$ (open squares) for the data taken with POI parallel to (a) *a*, (b) *b*, and (c) *c* principal axes, respectively. The $d^2\langle\varepsilon_1\rangle/dE^2$ and $d^2\langle\varepsilon_2\rangle/dE^2$ data are calculated as described in the text. For clarity, only 20% of the data points are shown. Energies of each CP structure are indicated by arrows and labeled in a numeric order.

Our SE-determined $\langle\varepsilon_{b2}\rangle$ spectrum (Fig. 4(d)) shows that the major optical absorption starts at ~1.3 eV, whereas the absorption onset in $\langle\varepsilon_{a2}\rangle$ and $\langle\varepsilon_{c2}\rangle$ spectra (Figs. 4(b) and 4(f)) seems to appear at slightly higher energy (~1.5 eV), which is consistent with some of the previously reported studies. Makinistian *et al.*[53] predicted maxima in the dielectric functions of 1.54 eV for the ε_{a2} and ε_{c2}, and 1.21 eV for the ε_{b2} (from semi-local DFT using a scissors operator). A room-temperature electro-reflectance study[54] also showed that the lowest direct gaps for the polarization of light parallel to the *a* and *b* axes are 1.6 and 1.3 eV, respectively. Our calculations confirm that SnS has a fundamental direct band gap at 1.22 eV regardless of the crystallographic orientations, as discussed earlier, but variation in optical transition intensity introduces the anisotropic response. This behavior will be important for PV applications in terms of deciding preferential material orientation and morphology, and in optical modeling for optimal device configurations.

In order to verify the theoretical prediction of the band gap at 1.22 eV, we perform the standard lineshape analysis[34,35] of the SE data, where the $\langle\varepsilon\rangle$ spectra are differentiated and smoothed numerically using algorithms of the Savitzky-Golay type,[55] followed by least-squares fitting of standard analytic CP expressions. The CP expressions are[56,57]

$$\frac{d^2\varepsilon}{dE^2} = \begin{cases} n(n-1)Ae^{i\phi}(E-E_g+i\Gamma)^{n-2}, & n \neq 0 \\ Ae^{i\phi}(E-E_g+i\Gamma)^{-2}, & n = 0, \end{cases} \quad (3)$$

where *A* is the amplitude, E_g is the threshold energy, Γ is the broadening parameter, and ϕ is the phase. The exponent *n* has values of -1, $-1/2$, 0, and $1/2$ for excitonic, one-, two-, and three-dimensional lineshapes, respectively. Real and imaginary parts are fit simultaneously.

Figures 5(a)–5(c) show the $d^2\langle\varepsilon\rangle/dE^2$ spectra (open symbols) together with the best-fit curves (lines) for the data taken with the POI parallel to the *a*, *b*, and *c* axes, respectively. A combination of two- ($n=0$) and three-dimensional ($n=1/2$) lineshapes is used to fit the data from 1.0 to 5.0 eV, which results in the minimum discrepancy between the data and fits. Energies of each CP structure are indicated by arrows and labeled in a numeric order. Differentiation substantially enhances the sensitivity to the weak optical structures, and multiple CP structures are now clearly seen. Even though presence of the optical transition at ~1.3 eV is not obvious in the $\langle\varepsilon_{a2}\rangle$ and $\langle\varepsilon_{c2}\rangle$ spectra shown in Figs. 4(b) and 4(f), it appears in the $d^2\langle\varepsilon_a\rangle/dE^2$ and $d^2\langle\varepsilon_c\rangle/dE^2$ spectra as a small shoulder. Inclusion of this transition in the lineshape analysis improved the quality of fits in the low-energy region of spectra. Unlike the case for $d^2\langle\varepsilon_a\rangle/dE^2$ and $d^2\langle\varepsilon_c\rangle/dE^2$ spectra, the $d^2\langle\varepsilon_b\rangle/dE^2$ spectrum shows a distinct optical structure at ~1.3 eV, which is indeed expected from Fig. 4(d).

The calculated and fit-determined CP energies are listed in Table II. The energy values reported in previous studies[32,53,54,58] are also included for comparison. For the ε_a and ε_b components, our data are in a good agreement with the results from previous studies. However, our data reveal two additional CP structures for those two light polarizations, and also provide the CP energies in SnS for the ε_c component that have not yet been obtained experimentally.

V. CONCLUSIONS

An experiment and theory combined study has been performed on the anisotropic optical properties of α-phase SnS. SE has been used to determine the ε_a, ε_b, and ε_c components of pseudo-dielectric-function tensor $\langle\varepsilon\rangle = \langle\varepsilon_1\rangle + i\langle\varepsilon_2\rangle$ spectra of α-SnS single crystal. The SE data clearly show a biaxial anisotropy in the optical properties of SnS, which is supported by the results of the calculated dielectric response from hybrid DFT. The calculations also predict that SnS possesses an indirect band gap of 1.11 eV and a direct gap of 1.22 eV for all three crystallographic orientations. Our SE data do not resolve the indirect band gap, but lineshape analysis of the second-energy-derivative of $\langle\varepsilon\rangle$ spectra reveals the direct band gap at ~1.3 eV. In addition to the direct band-gap onset, a total of eight above-band-gap critical-point (CP) structures were analyzed in the $d^2\langle\varepsilon\rangle/dE^2$ spectra in the spectral range of 1.0 to 5.0 eV. Probable electronic origin of each CP structure observed was identified based on the results from our hybrid DFT calculations. Our SE data

TABLE II. Fit-determined CP energies in eV for α-SnS. Calculated and previously reported CP energies are also included for comparison. Suggested symmetric points in Brillouin zone for each CP structure are listed.

CP	Theory—Symmetric points (k_x,k_y,k_z)	$\langle\varepsilon_a\rangle$	$\langle\varepsilon_b\rangle$	$\langle\varepsilon_c\rangle$
E_0	$1.11^{ind.}/1.22^{dir.}$	1.36,[a] 1.3[d]	1.31,[a] 1.21,[b] 1.3[c]	1.32[a]
E_1	1.87 – (0.0,0.0,0.0); Γ	1.59,[a] 1.54/1.6,[b] 1.6[c]	1.60,[a] 1.59[d]	1.61,[a] 1.54[b]
E_2	1.90 – (0.5,0.0,0.5); U	1.91[a]	1.98,[a] 1.91[d]	1.87[a]
E_3	1.97 – (0.0,0.0,0.5); Z	2.28,[a] 2.23,[b] 2.36,[d] 2.2[e]	2.34,[a] 2.35[d]	2.17[a]
E_4	2.45 – (0.0,0.5,0.0); Y	2.64,[a] 2.72[b]	2.76,[a] 2.72,[b] 2.80[d]	2.43,[a] 2.44[b]
E_5	3.08 – (0.5,0.5,0.0); S	2.98,[a] 2.82[d]	3.09[a]	2.84[a]
E_6	3.96 – (0.5,0.0,0.0); X	3.29,[a] 3.47,[b] 3.5[e]	3.42,[a] 3.41,[b] 3.56,[d] 3.3[e]	3.29[a]
E_7	5.23 – (0.5,0.5,0.5); R	3.71,[a] 3.93,[b] 3.7[d]	3.70,[a] 3.68[d]	3.64,[a] 3.99[b]
E_8	5.28 – (0.0,0.5,0.5); T	4.30,[a] 4.41,[d] 4.3[e]	4.06,[a] 4.17,[b] 4.5[e]	4.38,[a] 4.59[b]

[a]This work—Exp.
[b]Ref. 53—Theory.
[c]Ref. 54—Exp.
[d]Ref. 58—Exp.
[e]Ref. 32—Exp.

establish the optical function spectra of α-SnS in the three crystallographic orientations, which can be used as a reference for optical characterization of polycrystalline SnS thin films. The results from our comparison study of experimental data analysis and DFT calculations improve our understanding of the electronic structure of SnS. They highlight the strong anisotropic nature of this photo-active material and indicate that a SnS (001) terminated film is non-optimal crystal orientation for SnS-based photovoltaic devices.

ACKNOWLEDGMENTS

This work was supported by the U.S. Department of Energy as a part of the Non-Proprietary Partnering Program at the National Renewable Energy Laboratory under Contract No. DE-AC36-08-GO28308. A.W. acknowledges support from the Royal Society for a University Research Fellowship, and L.A.B. was funded by EPSRC (Grant No. EP/G03768X/1). Calculations were performed with the use of the IRIDIS High Performance Computing Facility, and associated support services at the University of Southampton.

[1]A. R. H. F. Ettema, R. A. de Groot, and C. Haas, Phys. Rev. B **46**, 7363 (1992).
[2]M. Devika, N. K. Reddy, K. Ramesh, R. Ganesan, K. R. Gunasekhar, E. S. R. Gopal, and K. T. R. Reddy, J. Elechem. Soc. **154**, H67 (2007).
[3]R. E. Banai, H. Lee, M. A. Motyka, R. Chandrasekharan, N. J. Podraza, J. R. B. Brownson, and M. W. Horn, IEEE J. Photovolt. **3**, 1084 (2013).
[4]A. Wangperawong, S. M. Herron, R. R. Runser, C. Hägglund, J. T. Tanskanen, H. B. R. Lee, B. M. Clemens, and S. F. Bent, Appl. Phys. Lett. **103**, 052105 (2013).
[5]J. L. Loferski, J. App. Phys. **27**, 777 (1956).
[6]P. Sinsermsuksakui, L. Sun, S. W. Lee, H. H. Park, S. B. Kim, C. Yang, and R. G. Gordon, "Overcoming Efficiency Limitations of SnS-Based Solar Cells," Adv. Energy Materials (published online).
[7]M. A. Green, K. Emery, Y. Hishikawa, W. Warta, and E. D. Dunlop, Prog. Photovolt.: Res. Appl. **22**, 1 (2014).
[8]P. Sinsermsuksakul, J. Heo, W. Noh, A. S. Hock, and R. G. Gordon, Adv. Energy Mater. **1**, 1116 (2011).
[9]L. A. Burton and A. Walsh, Appl. Phys. Lett. **102**, 132111 (2013).
[10]L. A. Burton, D. Colombara, R. D. Abellon, F. C. Grozema, L. M. Peter, T. J. Savenije, G. Dennler, and A. Walsh, Chem. Mater. **25**, 4908 (2013).
[11]J. Koh, H. Fujiwara, Y. Lu, C. R. Wronski, and R. W. Collins, Thin Solid Films **313–314**, 469 (1998).
[12]M. I. Alonso, M. Garriga, C. A. Durante Rincón, E. Hernández, and M. León, Appl. Phys. A **74**, 659 (2002).
[13]H. Fujiwara and M. Kondo, Phys. Rev. B **71**, 075109 (2005).
[14]M. A. Steiner, J. F. Geisz, I. García, D. J. Friedman, A. Duda, and S. R. Kurtz, J. Appl. Phys. **113**, 123109 (2013).
[15]M. Law, M. C. Beard, S. Choi, J. M. Luther, M. C. Hanna, and A. J. Nozik, Nano Lett. **8**, 3904 (2008).
[16]S. G. Choi, M. van Schilfgaarde, D. E. Aspnes, A. G. Norman, J. M. Olson, T. J. Peshek, and D. H. Levi, Phys. Rev. B **83**, 235210 (2011).
[17]S. G. Choi, H. Y. Zhao, C. Persson, C. L. Perkins, A. L. Donohue, B. To, A. G. Norman, J. Li, and I. L. Repins, J. Appl. Phys. **111**, 033506 (2012).
[18]S. G. Choi, J. Hu, L. S. Abdallah, M. Limpinsel, Y. N. Zhang, S. Zollner, R. Q. Wu, and M. Law, Phys. Rev. B **86**, 115207 (2012).
[19]S. G. Choi, R. Chen, C. Persson, T. J. Kim, S. Y. Hwang, Y. D. Kim, and L. M. Mansfield, Appl. Phys. Lett. **101**, 261903 (2012).
[20]Z. Zainal, M. Z. Hussein, and A. Ghazali, Sol. Energy Mater. Sol. Cells **40**, 347 (1996).
[21]S. Lopez and A. Ortiz, Semicond. Sci. Technol. **9**, 2130 (1994).
[22]F. G. Yanuar, F. Guastavino, C. Llinares, K. Djessas, and G. Masse, J. Mater. Sci. Lett. **19**, 2135 (2000).
[23]M. Calixto-Rodriguez, H. Martinez, A. Sanchez-Juarez, J. Campos-Alvarez, A. Tiburcio-Silver, and M. Calixto, Thin Solid Films **517**, 2497 (2009).
[24]N. K. Reddy and K. T. R. Reddy, Mater. Chem. Phys. **102**, 13 (2007).
[25]B. Ghosh, M. Das, P. Banerjee, and S. Das, Appl. Surf. Sci. **254**, 6436 (2008).
[26]O. E. Ogah, G. Zoppi, I. Forbes, and R. Miles, Thin Solid Films **517**, 2485 (2009).
[27]T. H. Sajeesh, N. Poornima, C. Sudha Kartha, and K. P. Vijayakumar, Phys. Status Solidi A **207**, 1934 (2010).
[28]J. Vidal, S. Lany, M. d'Avezac, A. Zunger, A. Zakutayev, J. Francis, and J. Tate, Appl. Phys. Lett. **100**, 032104 (2012).
[29]L. L. Cheng, M. H. Liu, M. X. Wang, S. C. Wang, G. D. Wang, Q. Y. Zhou, and Z. Q. Chen, J. Alloys Compd. **545**, 122 (2012).
[30]E. R. Shaaban, M. S. Abd El-Sadek, M. El-Hagary, and I. S. Yahia, Phys. Scr. **86**, 015702 (2012).
[31]H. R. Chandrasekhar, R. G. Humphreys, U. Zwick, and M. Cardona, Phys. Rev. B **15**, 2177 (1977).
[32]R. Eymard and A. Otto, Phys. Rev. B **16**, 1616 (1977).
[33]A. P. Lambros, D. Geraleas, and N. A. Economou, J. Phys. Chem. Solids **35**, 537 (1974).
[34]L. Viña, S. Logothetidis, and M. Cardona, Phys. Rev. B **30**, 1979 (1984).
[35]S. Zollner, M. Garriga, J. Humlícek, S. Gopalan, and M. Cardona, Phys. Rev. B **43**, 4349 (1991).
[36]T. Sorgenfrei, F. Hofherr, T. Jauß, and A. Cröll, Cryst. Res. Technol. **48**, 193 (2013).
[37]D. E. Aspnes, J. Opt. Soc. Am. **70**, 1275 (1980).
[38]G. E. Jellison, Jr. and J. S. Baba, J. Opt. Soc. Am. A **23**, 468 (2006).

[39]H. Fujiwara, *Spectroscopic Ellipsometry—Principles and Applications* (Wiley, West Sussex, 2007), Ch. 6 and 7.
[40]M. Schubert, in *Handbook of Ellipsometry*, edited by H. G. Tompkins and E. A. Irene (William Andrew, New York, 2005), Ch. 9.
[41]J. Heyd, G. E. Scuseria, and M. Ernzerhof, J. Chem. Phys. **124**, 219906 (2006).
[42]G. Kresse and J. Furthmuller, Phys. Rev. B **54**, 11169 (1996).
[43]G. Kresse and D. Joubert, Phys. Rev. B **59**, 1758 (1999).
[44]T. Chattopadhyay, J. Pannetier, and H. G. Von Schnering, J. Phys. Chem. Solids **47**, 879 (1986).
[45]S. P. Ong, W. D. Richards, A. Jain, G. Hautier, M. Kocher, S. Cholia, D. Gunter, V. Chevrier, K. A. Persson, and G. Ceder, Comput. Mater. Sci. **68**, 314 (2013).
[46]G. K. H. Madsen and D. J. Singh, Comput. Phys. Commun. **175**, 67 (2006).
[47]K. Momma and F. Izumi, J. Appl. Crystallogr. **44**, 1272 (2011).
[48]M. Gajdos, K. Hummer, G. Kresse, J. Furthmuller, and F. Bechstedt, Phys. Rev. B **73**, 045112 (2006).
[49]M. Parenteau and C. Carlone, Phys. Rev. B **41**, 5227 (1990).
[50]W. Albers, C. Haas, H. J. Vink, and J. D. Wasscher, J. Appl. Phys. **32**, 2220 (1961).
[51]O. Madelung, *Semiconductors: Data Handbook*, 3rd ed. (Springer, New York, 2004), p. 578.
[52]D. E. Aspnes, in *Handbook of Optical Constants of Solids*, edited by E. D. Palik (Academic, Orlando, 1985), Vol. I, p. 89.
[53]L. Makinistian and E. A. Albanesi, Phys. Status Solidi B **246**, 183 (2009).
[54]G. Valiukonis, D. A. Guseinova, G. Krivaité, and A. Sileika, Phys. Status Solidi B **135**, 299 (1986).
[55]A. Savitzy and M. J. E. Golay, Anal. Chem. **36**, 1627 (1964).
[56]M. Cardona, *Modulation Spectroscopy, Suppl. 11 of Solid State Physics* (Academic, New York, 1969), p 119.
[57]D. E. Aspnes, in *Handbook of Semiconductors*, edited by M. Balkanski (North-Holland, Amsterdam, 1980), Vol. 2, p. 109.
[58]F. Lukes, J. Humlicek, and E. Schmidt, Solid State Commun. **45**, 445 (1983).